Engineering lignin-derivable diacrylate networks with tunable architecture and mechanics

Yu-Tai Wong[1], LaShanda T. J. Korley[1,2]*

[1]Department of Chemical and Biomolecular Engineering, University of Delaware, Newark, Delaware 19716, United States

[2]Department of Materials Science and Engineering, University of Delaware, Newark, Delaware 19716, United States

*Corresponding author, E-mail: lkorley@udel.edu

1 ABSTRACT

Network engineering strategies offer a promising pathway toward tunable thermomechanical properties of bio-derivable, aromatic (meth)acrylate thermosetting polymers to expand their application library. In this work, a series of acrylate thermosets, synthesized from lignin-derivable vanillyl alcohol/bisguaiacol F diacrylates (VDA/BGFDA) and a bio-based *n*-butyl acrylate (BA), were designed as a sustainable platform to explore structure-architecture-property relationships. Using this approach, we examined a series of processable, fully bio-derivable vinyl ester resins while retaining comparable thermomechanical properties to conventional petroleum-based resins. Increasing the diacrylate content across all networks improved storage moduli at 25 °C (E'_{25}) by

up to 2 GPa (from 25 mol% to 75 mol% of diacrylate), and led to a more inhomogeneous network as evidenced by lower acrylate group conversion and a broader tan δ peak, indicating heterogeneous relaxation modes. Modifying the aromatic content of the starting diacrylate impacted the final inhomogeneity of the network, with increasing inhomogeneity observed for the bis-aromatic BGFDA relative to the mono-aromatic VDA. Similarly, combining the mono- and bis-aromatic diacrylates generated a network with a biphasic-like thermal relaxation mode. By correlating network architecture and material performance, the increasing architectural complexity suggested a more convoluted thermal relaxation mode while the enhancement of thermomechanical properties could still be achieved for potential application as damping materials. Overall, we presented a design strategy utilizing bio-derivable acrylates to expand the suite of renewable material platforms from a network engineering perspective.

Keywords: *Lignin-derivable, Diacrylates, Polymer networks, Vanillyl alcohol, Bisguaiacol, Thermomechanical properties, Network architecture, Renewable*

2 INTRODUCTION

Aromatic-based, thermosetting polymers are generally utilized in high-performance applications that require high mechanical strength, high glass transition temperatures (T_gs), and superior thermal stability due to their structural rigidity and dimensional stability.[1–7] Among various classes of thermosets, aromatic-based vinyl ester resins (*i.e.*, methacrylates and acrylates) are one of the most common polymer components in coatings and composites due to their high toughness and low cost.[1,8,9] Additionally, the relatively fast curing kinetics of vinyl ester resins paired with an appropriate formulation allows diverse processing techniques, such as liquid

molding and additive manufacturing.[8–10] However, current commercial precursors for aromatic vinyl ester resins are primarily petroleum-based with negative impacts on both human health and the environment. For example, bisphenol F (BPF) and bisphenol A (BPA), two widely used aromatic precursors for dental materials and commercial composites, are petroleum-derived and are known as human endocrine disruptors.[9,11–13] Moreover, vinyl ester resins usually contain a high concentration of reactive diluent (>40 wt%) to lower viscosities and increase the gel points for improved processability during curing. One of the most applied diluents, styrene, is sourced from petroleum resources and is a suspected volatile carcinogen.[8,9,14–17] Given these sustainability and safety hurdles, there is a pressing need to identify alternatives to petroleum-derived precursors with reduced toxicity and environmental impact.

To address these challenges in the development of high-performance polymeric materials, lignin serves as a promising replacement for petroleum feedstocks due to its aromatic structure, abundance in nature, and potentially lower toxicity.[1,18] Lignin exists in the cell walls of plants as a crosslinked biopolymer and is mostly underutilized as a by-product from the industrial pulping process.[18–21] More than 98% of this pulp waste is burned for energy recovery with a relatively low rate of valorization due to its complex and recalcitrant structure.[21] Although this unmodified lignin has been used in concrete fillers and composites, associated issues regarding unpleasant odors and dark colors limit the expansion of its applications.[22–24] Alternatively, lignin fractionation *via* cleaving β-O-4 linkages unravels numerous pathways to yield substituted phenols (*i.e.,* p-hydroxyphenyl, guaiacyl, and syringyl units), which can be further upgraded into various (bis)phenols through chemical modifications.[1,18,21] These (bis)phenols possess structural similarity to petroleum-derived counterparts with additional methoxy groups and other functional handles on the aromatic rings that can be leveraged to tune thermomechanical properties of the resultant

polymers.[1,2,18,19,25] From a toxicity perspective, lignin-derivable bisphenols (*i.e.,* bisguaiacols and bissyringols) exhibit lower estrogenic activity compared to petroleum-derived analogues, which is attributed to the additional methoxy groups that lower their binding affinity to estrogen receptors.[26,27] In addition to reduced health risks, lignin-derivable bisguaiacols have been reported to exhibit enhanced mechanical properties.[28] For example, introducing additional hydrogen bonding in a thermosetting non-isocyanate polyurethane (NIPU) system through inherent methoxy groups of bisguaiacols increased both elongation-at-break and toughness values of the final network.[28] The bio-derivable, crosslinked NIPUs also showcased similar network architecture to petroleum-derived systems even with the presence of additional methoxy groups as evidenced by comparable moduli.[28] Altogether, lignin-derivable (bis)phenolics provide a material platform for high-performance thermosets with improved renewability, lower health impacts, and comparable or even superior thermal and mechanical performance to their petroleum-derived counterparts.[8,28–36]

Over the past decade, lignin-derivable vinyl ester resins have gained increasing attention as viable replacements for petroleum-derived counterparts to achieve high-performance and promote sustainability.[1,8,14–16,37–39] Methacrylated lignin model compounds (*e.g.,* methacrylated vanillin, guaiacol, and eugenol) have been studied as substitutes for styrene as reactive diluents, reducing carcinogenic hazards and lowering volatilities due to the presence of the larger methacrylate group.[8,14–16,37] Resins incorporated with lignin-derivable methacrylates further exhibited comparable thermomechanical properties (*e.g.*, T_g and storage moduli) to those with styrene due to their structural similarity.[8,14–16,37] However, these bio-derivable methacrylates were observed to have higher viscosities, requiring additional reactive diluents to facilitate curing and thus hindering the direct replacement of traditional diluents in additive manufacturing and composites

applications.[8,39] To expand their application beyond diluents, Bassett et al. explored the substitution of petroleum-derived building blocks with lignin-derivable analogues to assess their potential to impart structural rigidity in performance-driven vinyl ester resins.[38] Despite the promising T_gs and moduli of these lignin-derivable dimethacrylates for high-performance applications, this study was limited to the use of petroleum-based reactive diluents (styrene) and only compared resins from different feedstocks.[38] To this end, this work aims to explore the design of processable vinyl ester resins utilizing lignin-derivable diacrylates with varying aromatic content and an aliphatic, bio-derivable acrylate as the reactive diluent for fully bio-derivable network formation.

Herein, the thermomechanical properties of a series of acrylate networks—photopolymerized through the reaction of lignin-derivable (bis)phenols (vanillyl alcohol or bisguaiacol F) diacrylates with a bio-derivable *n*-butyl acrylate (BA)—are investigated (**Scheme 1**). The chemistry and architecture of the final polymer are controlled using network engineering strategies by varying the diacrylate composition and the aromatic content of diacrylates to study the resulting structure-architecture-property relationships. Specifically, the effect of chemical composition on storage modulus (E'), tan δ, Young's modulus (E_t), and elongation-at-break (ε_b) are examined. The resulting network architectures and subsequent inhomogeneities are associated with 1) the final acrylate conversion, and 2) thermal transition modes, characterized by infrared spectra and the deconvolution study of tan δ curves, respectively. Through this design, we demonstrate a fully-renewable vinyl ester resin platform that utilizes lignin-derivable precursors to achieve high storage moduli and incorporates a bio-derivable aliphatic acrylate to enhance the resin processability. This research highlights the role of network engineering toward tunable

thermomechanical properties to expand the versatility of renewable vinyl ester resins for high-performance applications, ranging from coatings to composites.

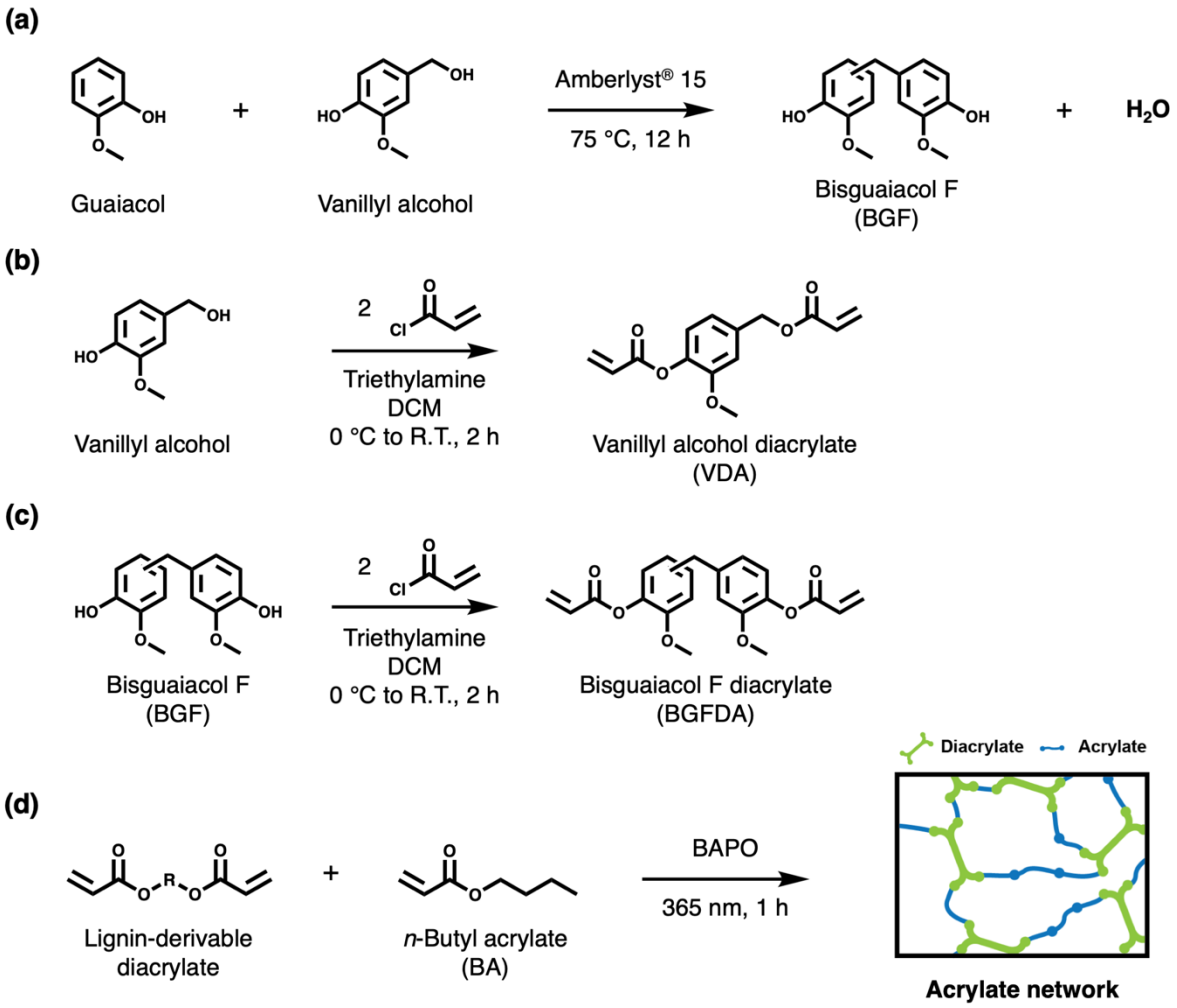

Scheme 1 Synthetic scheme of lignin-derivable diacrylates and acrylate networks. (a) Reaction of guaiacol and vanillyl alcohol to form bisguaiacol F (BGF). (b) Acrylation of vanillyl alcohol to yield vanillyl alcohol diacrylate (VDA). (c) Acrylation of BGF to yield bisguaiacol F diacrylate (BGFDA). (d) Photopolymerization to form acrylate networks with n-butyl acrylate (BA), where the diacrylate is either VDA, BGFDA, or a mixture of both.

3 EXPERIMENTAL

3.1 Materials

Dichloromethane (DCM; ≥ 99.5%), sodium bicarbonate (≥ 99.7%), sodium chloride (≥99.5%), hexanes (99%), ethyl acetate (≥99.5%), chloroform (>99.8%), and hydrochloric acid solution (36.5 to 38.0 wt%) were purchased from Fisher Scientific. Vanillyl alcohol, guaiacol (98%), Amberlyst® 15 hydrogen form (dry; MQ200), triethylamine, acryloyl chloride (≥97%), deuterated chloroform ($CDCl_3$; ≥99.9%) and phenylbis(2,4,6-trimethylbenzoyl)phosphine oxide (BAPO; 97%) were purchased from Sigma-Aldrich. *n*-Butylacrylate (BA; 99+%) was purchased from Acros Organics. BA was destabilized by passing through a basic alumina column before use. All chemicals except for BA were used as received.

3.2 Synthesis of bisguaiacol F (BGF)

BGF was synthesized as described in the literature (**Scheme 1a**).[28,29] Vanillyl alcohol (0.03 mol, 5 g) and guaiacol (0.13 mol, 16 g) were added into a single-neck round-bottom flask equipped with a magnetic stir bar. The reaction mixture was stirred and heated at 75 °C with an Ar sparge for 40 min. The solid catalyst, Amberlyst® 15 hydrogen form (1.5 g, 30% w/w relative to vanillyl alcohol), was subsequently added to the reaction mixture. The reaction proceeded for 12 h. The reaction mixture was then cooled to ~20 °C and dissolved in ~50 mL of DCM. The solid catalyst was removed by filtration. The filtrate was washed with ~50 mL of deionized (DI) water three times in a separatory funnel. The organic phase was collected, and excess DCM was removed by rotary evaporation. The residue was further purified by automated flash column chromatography (Biotage® Selekt, Sfär Silica Column—60 μm particle size, 100 Å pore size, 100 g silica gel) with a step gradient of ethyl acetate (33% v/v) and hexanes (67% v/v) as the mobile phase. The collected product was concentrated by rotary evaporation, and further dried in a vacuum oven at 25 °C for

12 h to yield BGF as a white solid (purity: >99%, yield: ~54 mol%). Proton (^{1}H) Nuclear Magnetic Resonance (NMR) (600 MHz, $CDCl_3$) δ 6.85-6.64 (m, 6H), 5.48 (s, 2H), 3.85-3.83 (m, 8H). Fourier Transform Mass Spectrometry (FTMS) (Electrospray Ionization [ESI], *m/z*): calculated for $C_{15}H_{16}O_4$ 260.1049; found 260.1041. The ^{1}H NMR spectrum with peak assignments is shown in **Fig. S1**.

3.3 General procedure for the synthesis of diacrylates

In a typical diacrylate synthesis, 1 eq. of alcohol (vanillyl alcohol or BGF), 4 eq. of triethylamine, and 0.3 M (relative to alcohol) of DCM were added into a single-neck round-bottom flask equipped with a magnetic stir bar. The reaction mixture was stirred and sparged with Ar for 40 min in an ice bath. Under Ar flow, 3 eq. of acryloyl chloride was added dropwise into the reaction mixture, and the reaction was warmed back to ~20 °C followed by proceeding for 2 h. Next, the solution was concentrated by rotary evaporation to remove DCM, and the residue was dissolved in ethyl acetate. The solution mixture was subsequently washed sequentially in: 1) 1 m HCl solution, 2) saturated sodium bicarbonate solution, and 3) saturated brine in a separatory funnel. The organic phase was collected, and excess ethyl acetate was removed by rotary evaporation. Both diacrylates were purified by automated flash column chromatography (Biotage® Selekt, Sfär Silica Column—60 µm particle size, 100 Å pore size, 100 g silica gel) with a step gradient of ethyl acetate (33% v/v) and hexanes (67% v/v) as the mobile phase. The diacrylates were recovered and dried at ~ 20 °C under vacuum to afford white solids.

VDA. White solid (purity: >99%, yield: ~50%). ^{1}H NMR (600 MHz, $CDCl_3$) δ 7.07 (d, J = 8.0 Hz, 1H), 7.02-6.96 (m, 2H), 6.61 (dd, J = 17.3, 1.3 Hz, 1H), 6.46 (dd, J = 17.3, 1.4 Hz, 1H), 6.35 (dd, J = 17.3, 10.5 Hz, 1H), 6.18 (dd, J = 17.3, 10.4 Hz, 1H), 6.01 (dd, J = 10.5, 1.3 Hz, 1H), 5.87

(dd, J = 10.4, 1.3 Hz, 1H), 5.18 (s, 2H), 3.84 (s, 3H). FTMS (ESI, *m/z*): calculated for $C_{14}H_{14}O_5$ 262.2386; found 263.0924. The ^{1}H NMR spectrum with peak assignments is shown in **Fig. S2**.

BGFDA. Light yellow solid (purity: >99%, yield: ~43 mol%). ^{1}H NMR (600 MHz, $CDCl_3$) δ 7.05-6.96 (m, 2H), 6.94-6.69 (m, 4H), 6.60 (ddd, J = 17.4, 4.1, 1.3 Hz, 2H), 6.39-6.29 (m, 2H), 6.02-5.97 (m, 2H), 3.95 (d, J = 30.2 Hz, 2H), 3.85-3.69 (m, 6H). FTMS (ESI, *m/z*): calculated for $C_{21}H_{20}O_6$ 368.3516; found 369.1321. The ^{1}H NMR spectrum with peak assignments is given in **Fig. S3**.

3.4 BA (purchased)

^{1}H NMR (600 MHz, $CDCl_3$) δ 6.33 (dd, J = 17.3, 1.5 Hz, 1H), 6.06 (dd, J = 17.4, 10.4 Hz, 1H), 5.74 (dd, J = 10.5, 1.5 Hz, 1H), 4.10 (t, J = 6.7 Hz, 2H), 1.64-1.56 (m, 2H), 1.40-1.30 (m, 2H), 0.89 (t, J = 7.4 Hz, 3H). FTMS (ESI, *m/z*): calculated for $C_7H_{12}O_2$ 128.1588; found 129.0903. The ^{1}H NMR spectrum with peak assignments is given in **Fig. S4**.

3.5 Preparation of acrylate networks

All diacrylate networks were prepared *via* radical photopolymerization by reacting diacrylate and acrylate in different compositions with BAPO as the photoinitiator (1% w/w relative to the monomer mixture) under ambient conditions. Due to the solid form of both VDA and BGFDA at room temperature and their varying solubility in the BA, VDA/BA networks were cured in bulk with 25, 50, and 75 mol% of diacrylate, while BGFDA/BA networks were cured with 25 and 50 mol% of diacrylate. Herein, materials formed can be denoted as follows: A/B(/C)-X/Y(/Z), where A, B, and C refer to the monomer used, and X, Y, and Z refer to the mol% of the monomer on a molecule basis. It also was noted that the two acrylate groups of VDA can differ in reactivity depending on whether the ester oxygen is connected to a benzyl or a phenyl group, which will be discussed in a later section.

The fabrication procedure for VDA/BA-75/25 is detailed as an example. To a scintillation vial, VDA (0.86 g, 3.28 mmol), BA (0.14 g, 1.09 mmol), and BAPO (10 mg, 2.4×10^{-2} mmol) were dissolved in 5 mL of DCM, and mixed by shaking on a shaker plate at 600 rpm for 10 min, with the vial covered in aluminum foil to prevent early initiation until complete solubilization. The solution was then poured into a PTFE evaporating dish having dimensions of 12 mm × 65 mm (height × diameter), and covered to prevent early termination of the photoinitiator. After the complete evaporation of DCM for 24 h, the film was cured in an ultraviolet (UV) chamber (SPDI UV, $\lambda = 365$ nm) at an intensity ~13 $mW \cdot cm^{-2}$ for 1 h and followed by a thermal post-curing at 150 °C for additional 24 h to ensure maximum conversion (**Fig. S5** and **S6**). The temperature for thermal post-curing after photopolymerization was determined by the exothermic peaks in differential scanning calorimetry (DSC) (**Fig. S7**). Rectangular films were then cut from the bulk film after thermal post-curing to provide specimens having dimensions of 200 mm × 3 mm × 0.2 mm (length × width × thickness) for further characterization.

3.6 Soxhlet extraction

After network formation, the gel fraction was probed *via* Soxhlet extraction. Samples were weighed to obtain the initial mass (m_0) before the extraction. The extraction was then completed for 24 h with a single cycle duration ~15 min at 90 °C using ~250 mL of chloroform as the extraction solvent. Samples were subsequently dried in a vacuum oven at ~20 °C for 24 h and weighed to obtain the dry mass (m_{dry}). The gel fraction was estimated as m_{dry}/m_0. Soxhlet extraction was performed three times on each sample, and the reported values are the average gel fraction with the error reported as a standard deviation.

3.7 ^{1}H NMR spectroscopy

All NMR samples were prepared in $CDCl_3$ and analyzed using a Bruker AVANCE III 600 MHz (5-mm SMART probe) spectrometer. Processing and analysis of ^1H NMR spectra was completed using the MestReNova software package.

3.8 Mass spectrometry

The masses of BGF, lignin-derivable diacrylates, and BA were measured by ESI-FTMS using a Q-Exactive Orbitrap (Thermo Fisher Scientific) mass spectrometer. Prior to the analysis, samples were dissolved in DCM at a concentration of 0.1 $mg \cdot mL^{-1}$. Direct syringe injection of the samples into the mass spectrometer was conducted in a positive ion mode for ESI-FTMS.

3.9 Attenuated total reflectance- Fourier transform infrared (ATR-FTIR) spectroscopy

ATR-FTIR spectroscopy was performed using a Thermo Nicolet NEXUS 870 FTIR with a deuterated triglycine sulfate/potassium bromide (DTGS/KBr) detector. All acrylate network films were scanned (128 scans) at a resolution of 4 cm^{-1} in the wavenumber range of 400–4000 cm^{-1}. Network conversion was assessed by the examination of the acrylate double bond stretching band at ~1635 cm^{-1} and carbonyl stretching band at ~1724 cm^{-1} as an internal reference (**Fig. S8**) by Eq. (1):

$$\text{Conversion}(t) = \frac{[\frac{h_{1635}}{h_{1724}}]_0 - [\frac{h_{1635}}{h_{1724}}]_t}{[\frac{h_{1635}}{h_{1724}}]_0} \times 100 \quad \text{(Eq. 1)}$$

where $[\frac{h_{1635}}{h_{1724}}]_0$ and $[\frac{h_{1635}}{h_{1724}}]_t$ are the ratios before and after UV exposure for time *t*, respectively, between the height of the acrylate double bond stretching band (~1635 cm^{-1}) and the internal reference (~1724 cm^{-1}). Reported conversions are an average of individually triplicate measurements with errors representing standard deviations.

3.10 Differential scanning calorimetry (DSC)

DSC (Discovery DSC, TA Instruments) was employed to examine the additional curing peaks after UV curing of acrylate networks. Each sample was encapsulated in a T_{zero} aluminum pan sealed with the corresponding hermetic lid. Two heating/cooling cycles were performed between 0 and 250 °C under a continuous N_2 flow (50 mL·min^{-1}) at a rate of 10 °C·min^{-1}. The temperature corresponding to the maximum of the exothermic peak was identified as an additional curing temperature. DSC curves are presented in **Fig. S7**.

3.11 Thermogravimetric analysis (TGA)

TGA (Discovery TGA, TA Instruments) was used to study the thermal stability of acrylate networks. Each sample was placed in a 100 μL platinum pan. All samples were heated to 700 °C from ~20 °C at a heating rate of 10 °C·min^{-1} under a continuous N_2 flow (50 mL·min^{-1}). The temperature at 5 wt% loss ($T_{d,5\%}$) was used to assess the thermal stability of crosslinked acrylate networks. TGA curves are presented in **Fig. S9** and summarized in **Table S1**.

3.12 Dynamic mechanical analysis (DMA)

An RSA-G2 Solids Analyzer (TA Instruments) was used to determine the storage modulus (*E'*), loss modulus (*E"*), and tan δ (*E"/E'*) of each specimen using oscillatory tension mode with a strain amplitude of 0.075%, frequency of 1 Hz, and an axial force of 0.4 N. Rectangular samples were first heated to 250 °C, and then cooled to -100 °C followed by a heating cycle to 250 °C at a rate of 3 °C·min^{-1}. Data from the final heating trace were used for analysis. Reported moduli and tan δ are an average of individually triplicate measurements with errors representing standard deviations.

3.13 Tensile testing

Tensile properties of the acrylate networks were measured on a Zwick/Roell tensile tester with a load cell of 100 N and a clamp force of 200 N at ~20 °C. Rectangular samples were subjected

to an extension rate of 10%·min^{-1} until film breakage. The ultimate tensile strength (σ_m), elongation-at-break (ε_b), Young's modulus (E_t), and toughness results are reported as an average of triplicate measurements with errors representing standard deviations.

3.14 Small-angle X-ray scattering

SAXS data were collected using a Xenocs Xeuss 2.0. X-rays were generated at 50 kV/0.6 mA at a beam wavelength of 1.542 Å (Cu Ka radiation) and a sample-to-detector distance of 1200 mm. The scattered beam was recorded on a CCD detector with a pixel resolution of 172 × 172 mm. 2D patterns were azimuthally integrated to obtain the scattering intensity as a function of the absolute value of the scattering vector, $Q = \left|\vec{Q}\right| = 4\pi\lambda^{-1}\sin\theta$, where λ and θ denote the wavelength of the X-ray beam and the half of the scattering angle, respectively.

4 RESULTS AND DISCUSSION

The aromatic nature of lignin-derivable (bis)phenols diacrylates suggested their potential in imparting rigidity to high-performance vinyl ester networks designed with renewable feedstocks. Meanwhile, the incorporation of a bio-derivable, aliphatic acrylate with low viscosity can further facilitate resin processability and serve as a precursor for network engineering. The combination of a rigid crosslinker (*e.g.,* VDA, BGFDA) and a flexible spacer (*i.e.,* BA) allowed modulation of the network chemistry and architecture by controlling diacrylate compositions and the aromatic content of the diacrylate (monophenol vs. bisphenol) toward tunable thermomechanical properties. To examine this network engineering strategy, two lignin-derivable (bis)phenols, vanillyl alcohol and BGF, were acrylated through the nucleophilic reaction with acryloyl chloride, respectively, to form diacrylates (VDA and BGFDA, **Scheme 1b and 1c**), while BGF was synthesized *via* the acid-catalyzed electrophilic aromatic substitution between guaiacol and vanillyl alcohol as

reported (**Scheme 1a**).[28,29] Bio-derivable BA was chosen as the reactive diluent to control the distance between junction points due to its low viscosity and aliphatic structure that provides extra flexibility to networks. All networks were subsequently prepared *via* bulk free-radical photopolymerization using either VDA or BGFDA as the crosslinker and BA as the reactive diluent. Compositions of diacrylate ranged from 25 mol% to 75 mol% depending on the solubility of diacrylate in BA to investigate the connection between network chemistry, architectural features, and thermomechanical properties. In addition to two-component networks, we also investigated a mixed diacrylate system using an equal amount of VDA and BGFDA (*i.e.*, VDA/BGFDA/BA-25/25/50) to compare the effect of aromatic content of diacrylate within two-component networks (VDA/BA-50/50 and BGFDA/BA-50/50).

Preparation of acrylate networks

All network formations were monitored by ATR-FTIR for the disappearance of the acrylate alkene stretching band at ~1635 cm^{-1}, and subsequently conversions were quantified using Eq. (1). Unreacted groups were present in all cases, indicated by the incomplete conversion (final conversion <100%, **Table 1)** due to the decreased chain mobility after gelation, which inhibits pendent acrylate groups from reacting.[40] Increasing the content of aromatic diacrylate led to earlier local gelation, which hindered the mobility of reactive groups to diffuse and react with each other as noted by the drop in final conversions from 92.4% to 61.6% in VDA/BA networks, and 86.6% to 78.7% in BGFDA/BA networks. However, the final conversions of BGFDA/BA networks were slightly lower than VDA/BA networks (~4–6% lower) when a similar amount of diacrylate was used. This lower conversion is possibly caused by the higher observed viscosity of the BGFDA/BA resins during formulation preparation, subsequently reducing the mobility and propagation of reactive groups as reported in earlier studies.[40] Notably, the network with mixed diacrylates

(VDA/BGFDA/BA-25/25/50) exhibited the lowest conversion (~73.1%) compared to the single diacrylate networks (82.3% of VDA/BA-50/50 and 78.7% of BGFDA/BA-50/50**)**. It also was noted that conversions of these three networks were all within the range of error, indicating no significant difference in final conversions was observed after post-curing, and the slight variation between these networks was potentially driven by the viscosity of the resin solution. The gel fractions of all networks were over 95% in all cases (**Table 1**), demonstrating that the networks are highly crosslinked. To highlight the evolution of network formation using lignin-derivable diacrylates, a conversion profile under different curing times for the VDA/BA networks is detailed in **Fig S10**. Conversions were obtained at cure times of 15, 30, 45, and 60 min, and after thermal post-curing. All VDA/BA networks approached their maximum extent of curing within 30 min, highlighting the fast curing kinetics and also the inevitable formation of pendant groups in highly-crosslinked networks.

Table 1 Final conversion and gel fraction of acrylate networks

Sample	Final conversion (%)[a]	Gel fraction (%)[b]
VDA/BA-25/75	92.4 ± 0.4	95.7 ± 2.3
VDA/BA-50/50	82.3 ± 7.4	99.9 ± 0.1
VDA/BA-75/25	61.6 ± 11.8	99.9 ± 0.1
BGFDA/BA-25/75	86.6 ± 4.8	98.2 ± 2.1
BGFDA/BA-50/50	78.7 ± 10.4	97.7 ± 4.0
VDA/BGFDA/BA-25/75	73.1 ± 2.8	99.9 ± 0.1

[a] Determined by ATR-FTIR using the disappearance of the acrylate C=C peak (~1635 cm^{-1}) after thermal post-curing at 150 °C. [b] Determined by Soxhlet extraction with chloroform as the extraction solvent.

Thermomechanical properties of acrylate networks

The thermomechanical properties of acrylate networks were examined by DMA and are summarized in **Table 2**. The storage moduli at 25 ºC (E'_{25}) and 200 ºC (E'_{200}) were used to approximate the moduli in the glassy and rubbery states, respectively. However, it also should be noted that all networks showed no distinct glassy and rubbery state reflected in the shape of *E'* curves (**Fig. 1**), which is an indication of the inhomogeneity that will be discussed in the next section.

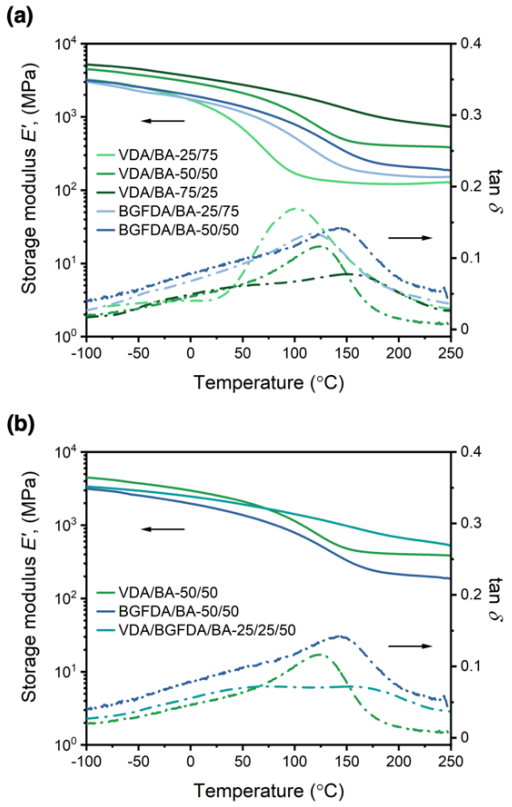

Fig. 1 Storage modulus (solid line, -) and tan δ (dashed line, --) as a function of temperature for (a) varying diacrylate content and (b) varying diacrylate type with a total diacrylate content at 50 mol%.

Overall, the composition of diacrylate in the network dictates the value of E'_{25} and E'_{200} as shown in **Fig. 1a**. For example, E'_{25} for VDA/BA networks was enhanced from ~1.1 GPa to 3.1 GPa by increasing the VDA content from 25 mol% to 75 mol%, and E'_{25} for BGFDA/BA networks shifted slightly from ~1.5 GPa to 1.7 GPa by increasing the BGFDA amount from 25 mol% to 50 mol%. Similarly, E'_{200} for VDA/BA was enhanced from ~0.1 GPa to 0.9 GPa by increasing VDA content from 25 mol% to 75 mol%, and E'_{200} for BGFDA/BA remained similar at ~0.2 GPa with BGFDA content increasing from 25 mol% to 50 mol %. This trend in *E'* was likely the result of a denser network resulting from the incorporation of a higher diacrylate content. Additionally, the transition of *E'* from a glassy to rubbery state becomes less apparent with increasing diacrylate content, suggestive of restricted chain mobility triggered by temperature change, when a denser network is obtained.[41,42] Beyond the *E'* tunability of VDA/BA and BGFDA/BA networks, these bio-derivable networks also showed comparable E'_{25} (ranging from 1~3 GPa) to petroleum-derived, commercial (meth)acrylate thermosets with E'_{25} in the range of 2~3 GPa.[1,40]

Table 2 Thermomechanical properties of acrylate networks

Sample	E'_{25} (GPa) [ab]	E'_{200} (GPa) [ab]	E_t (MPa) [cd]	ε_b (%) [d]
VDA/BA-25/75	1.1 ± 0.4	0.1 ± 0.1	1.3 ± 0.1	4.3 ± 1.6
VDA/BA-50/50	2.6 ± 0.3	0.4 ± 0.1	2.0 ± 0.4	1.6 ± 0.3
VDA/BA-75/25	3.1 ± 0.2	0.9 ± 0.1	2.0 ± 0.8	1.9 ± 0.4
BGFDA/BA-25/75	1.5 ± 0.3	0.2 ± 0.1	0.8 ± 0.2	4.4 ± 0.2
BGFDA/BA-50/50	1.7 ± 0.4	0.2 ± 0.1	1.5 ± 0.1	1.8 ± 0.3
VDA/BGFDA/BA-25/25/50	2.2 ± 0.1	0.7 ± 0.1	1.4 ± 0.1	2.3 ± 0.

[a] Reported values are the average of triplicate measurements with errors representing standard deviations. [b] Determined from the second heating trace of DMA experiments in oscillatory film tension mode at a heating rate of 3 °C, strain amplitude of 0.075%, frequency of 1 Hz, and an axial force of 0.4 N. [c] Young's modulus was determined from the slope of the initial elastic region in the engineering tensile stress-strain curves. [d] All data are based on tensile stress-strain curves obtained from the uniaxial tensile testing using a loading cell of 100 N and an extension rate of 10%/min at ~20 °C. Each measurement is triplicated with errors representing standard deviations.

The trend of *E'* is more complex when comparing networks with varying diacrylate type while maintaining the total diacrylate content at 50 mol% (**Fig. 1b**). BGFDA/BA network exhibited the lowest *E'* throughout the temperature range (E'_{25} ~1.7 GPa and E'_{200} ~0.21 GPa), whereas VDA/BA network had the highest E'_{25} (~2.6 GPa) and an intermediate E'_{200} (~0.40 GPa). Interestingly, the network with mixed diacrylates, VDA/BGFDA/BA-25/25/50, showed an intermediate E'_{25} (~2.2 GPa) and the highest E'_{200} (~0.68 GPa). The lower E'_{25} and E'_{200} of BGFDA/BA was likely due to the larger diacrylate unit leading to a slightly looser network. However, the response of *E'* to temperature change for the VDA/BGFDA/BA-25/25/50 network suggested a network with a higher content of various architectural features, including unreacted groups and clusters of crosslinks, that induce chain motion across a wider range of temperature.[43]

Unlike conventional thermosets, distinct glass transition temperatures (T_gs) were unable to be identified using the tan δ curves for these highly-crosslinked networks due to the broad nature of the transition. While tan δ is defined as the ratio between viscosity and elasticity indexes (*E''*/*E'*), the peak is commonly applied as an indication of glass transition behavior. However, we observed that width of the tan δ peaks increased as the diacrylate content increased (**Fig. 1a**). The

flattening and broadening of tan δ curves with increased diacrylate content suggested a more inhomogeneous network, leading to complex thermal relaxation modes.[41,42,44,45]

Network inhomogeneity and architecture

Defects, such as loops and unreacted groups, inevitably arise during free-radical crosslinking process due to the interplay between reaction kinetics and diffusion limits.[44] These molecular-scale defects are further encompassed in a non-uniform spatial distribution of crosslinking junctions and subsequently dictate the network architecture and thermomechanical performance.[44,46] In this work, we anticipated that unreacted groups and non-uniform spatial distribution of junctions would dominate the inhomogeneous nature of our networks because loops are less likely to occur in concentrated gels, such as a bulk polymerization.[47–49] To investigate the occurrence of these architectural features, unreacted groups were characterized by conversion studies, and tan δ curves from DMA that reflect the thermal response of chain motions were examined to semi-quantitatively determine the overall inhomogeneity. Interestingly, these bio-derivable acrylate networks exhibited broad tan δ curves, which are one of the essential features for damping materials.[50] The broad tan δ curves are likely a result of the formation of microphases, and prompted the exploration of microscopic network architecture of these bio-derivable acrylate networks *via* deconvolution of tan δ curves into Gaussian peaks (**Fig. 2**).[51] Each deconvoluted Gaussian peak was treated as a microphase with relaxation temperatures corresponding to a distinct chemical composition and architecture embedded within the bulk network. The tan δ curves of these networks can be deconvoluted into 3-4 Gaussian bands, which are summarized in **Table 3**. Based on the peak positions, we further assigned these relaxation bands to different compositions in the order of increasing temperature to phases of BA, BA-rich, diacrylate-rich, and diacrylate. Notably, the assignments of deconvoluted peaks at the lowest temperature was supported by the

reported T_g for poly(*n*-butyl acrylate**)** at ~-50 ºC, and peaks at the highest temperature were consistent with estimated T_gs for VDA and BGFDA homopolymers at ~190 and 220 ºC, respectively, as determined by the polymer properties prediction website, Polymer Genome (**Fig. S11**).[52–54] These deconvoluted peaks also are quite broad with a maximum peak width spanning over 200 ºC, indicating the inhomogeneous nature of each microphase themselves. These microphases comprised micro-structured defects, including unreacted groups and junction clusters, which were unobservable by small-angle X-ray scattering (*i.e.,* no apparent peaks were observed, **Fig. S12**).

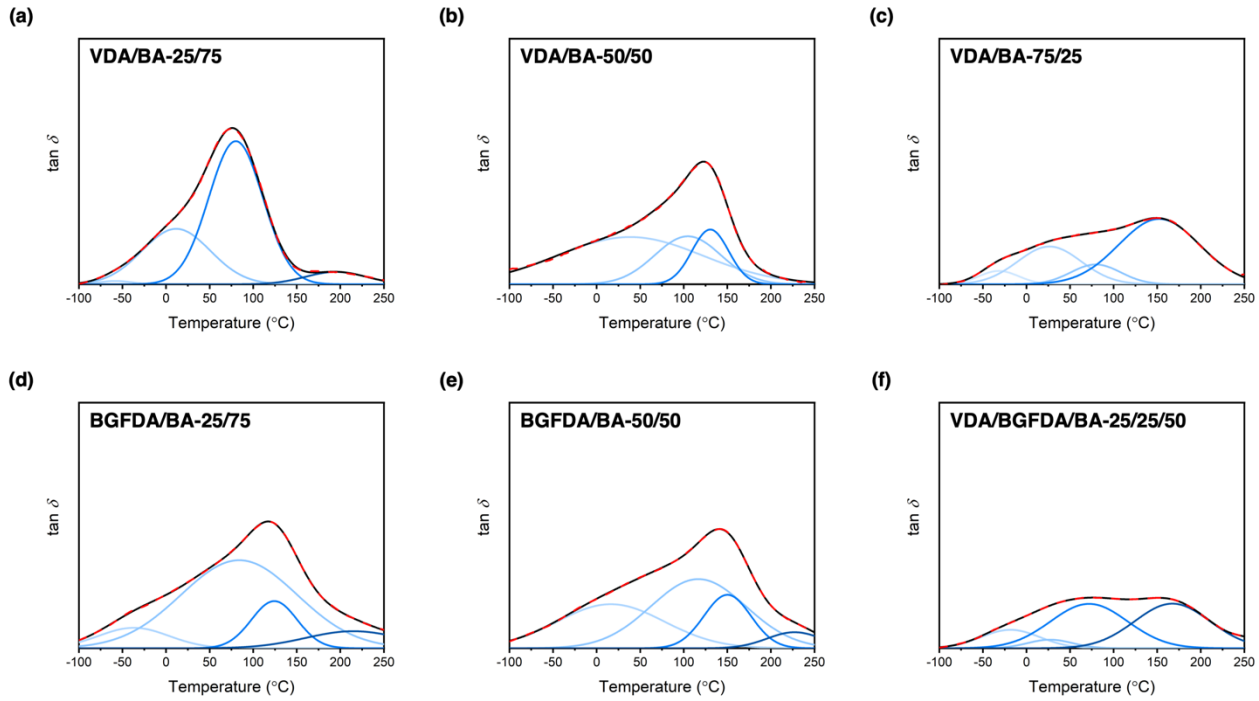

Fig. 2 Deconvolution of tan δ curves of acrylate networks. The red dashed line (--) denotes the original curve, and the black solid line (-) is the integrated result of deconvoluted curves. All y-axes are on the same scale.

As detailed in **Table 3**, no distinct trends in each microphase were revealed by the deconvolution studies. Alternatively, the height and position of the maximum tan δ peaks were examined to determine the network structure and overall inhomogeneity. Increasing the diacrylate content resulted in shifts of both the maximum tan delta peak and the dominant deconvoluted peak to higher temperatures, indicating a denser network structure with the incorporation of more crosslinker. For example, the maximum tan δ peak for VDA/BA networks shifted from ~77 ºC to ~151 ºC when increasing the VDA content from 25 mol% to 75 mol%, and the peak for BGFDA/BA networks shifted from ~119 ºC to ~143 ºC when the BGFDA content was increased by 25 mol%. The height of the maximum tan δ peak was reduced when a higher content of diacrylate was incorporated, indicating increased inhomogeneity with microphases more evenly relaxing over a wide range of temperature for both VDA/BA and BGFDA/BA networks.

Table 3 Deconvolution results of acrylate networks

Sample	Max tan δ temperature (°C)	Phase 1		Phase 2		Phase 3		Phase 4	
		Center (°C)	FWHM (°C)[a]	Center (°C)	FWHM (°C)[a]	Center (°C)	FWHM (°C)[a]	Center (°C)	FWHM (°C)[a]
VDA/BA-25/75	77	-58	44	11	92	80	85	195	81
VDA/BA-50/50	123	-	-	38	197	105	99	130	54
VDA/BA-75/25	151	-32	54	26	86	80	67	152	109
BGFDA/BA-25/75	119	-37	94	84	157	124	85	215	N.A.
BGFDA/BA-50/50	143	16	144	117	129	150	63	227	N.A.

VDA/BGFDA/BA-25/25/50	78 154	-18	79	27	60	72	104	167	102

[a] Determined as the full width at half maximum (FWHM) of the deconvoluted curve.

Varying the diacrylate type (*i.e.,* VDA, BGFDA, or a mix of VDA and BGFDA) had a more complex connection to the thermomechanical behavior because the size of the diacrylate unit and reaction kinetics need to be considered simultaneously. VDA/BA-50/50 exhibited a slightly higher maximum tan δ peak temperature than BGFDA/BA-50/50 (123 ºC vs. 119 ºC), which is potentially caused by the larger BGFDA unit leading to a slightly looser network. However, BGFDA/BA-50/50 showed a higher extent of inhomogeneity with a more pronounced shoulder peak at the lower temperature range (0 ~ 50 ºC), agreeing with the trend of more unreacted groups resulted from a higher resin viscosity. The higher extent of inhomogeneity exhibited by BGFDA/BA networks indirectly suggests that the reactivity of the two acrylate groups of VDA isn't significantly different. In contrast, a notable difference in the reactivity would likely result in a more inhomogeneous network characterized by the presence of non-uniformly distributed junction clusters. Surprisingly, the network with mixed diacrylates (VDA/BGFDA/BA-25/25/50) showed a biphasic-like thermal transition with two prominent microphases at 72 ºC and 167 ºC. The VDA/BGFDA/BA network displayed a more inhomogeneous network compared with VDA/BA and BGFDA/BA networks despite having an intermediate aromatic content. This result is likely due to the different reactivities between VDA, BGFDA, and BA that impart more complexity to the reaction kinetics, which require future investigation.

Overall, increased inhomogeneity was observed with increasing diacrylate content or by changing the diacrylate from monophenol (VDA) to bisphenol (BGFDA), agreeing with expected influence of unreacted groups. A schematic representation of the impact of diacrylate content and

aromatic content of diacrylate is summarized in **Fig. 3**. The increase in *E'* and the broad tan δ curves can be further leveraged for damping applications despite the network inhomogeneity.

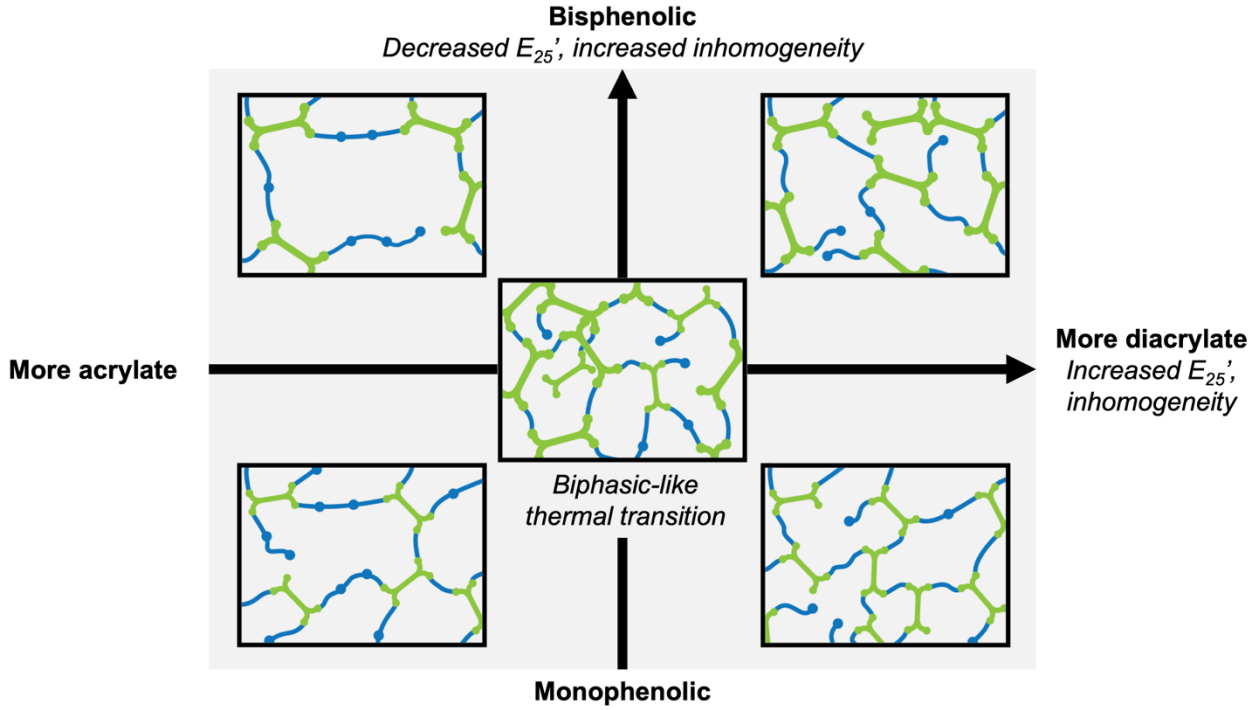

Fig. 3 Schematic representation of the effect of network architecture on thermomechanical properties.

Tensile properties of acrylate networks

The mechanical behavior of each network was examined through uniaxial tensile testing to probe the influence of network architectures on Young's modulus (E_t) and elongation-at-break (ε_b) (**Fig. 4**). Similar to the trend of *E'*, increasing the diacrylate content enhanced E_t as a result of a denser network (**Fig. 4a**), where the E_t of VDA/BA-50/50 was ~0.74 GPa higher than VDA/BA-25/75 (2.04 GPa vs. 1.30 GPa, **Table 2**), and E_t of BGFDA/BA-50/50 was ~0.71 GPa higher than BGFDA/BA-25/75 (1.48 GPa vs. 0.77 GPa). However, the E_t values of VDA/BA-75/25 (1.96 ±

0.77 GPa) and VDA/BA-50/50 (2.04 ± 0.42 GPa) were not significantly different, indicating the elastically ineffective junctions from inhomogeneity start to dictate the tensile properties with higher diacrylate content. Furthermore, VDA/BA-50/50 showed the highest E_t value among the networks when varying diacrylate types due to the smaller diacrylate unit leading to a denser structure, while BGFDA/BA and VDA/BGFDA/BA have similar E_t within error (1.48 ± 0.11 GPa vs. 1.42 ± 0.10 GPa, respectively).

Unsurprisingly, the acrylate networks were mechanically brittle (ε_b < 5% and toughness < 1.06 MJ m^{-3}, **Table S2**) due to their highly crosslinked structure. In contrast to the trend of E_t, increasing the diacrylate content led to a reduction in ε_b (**Fig. 4b**) with a denser network limiting network extensibility. As with E_t, ε_b values of VDA/BA-75/25 and VDA/BA-50/50 were statistically the same (1.60 ± 0.26% vs. 1.90 ± 0.42%), which can similarly be attributed to the pronounced presence of elastically ineffective junctions due to inhomogeneities at high diacrylate content. Interestingly, networks using 50 mol% of diacrylate showed ε_b ~2%, while VDA/BGFDA/BA has a slightly higher ε_b. This finding agreed with a previous study that concluded that brittle networks show no significant impact on ε_b as the extent of inhomogeneity increases; ε_b is mainly dictated by the diacrylate content.[55]

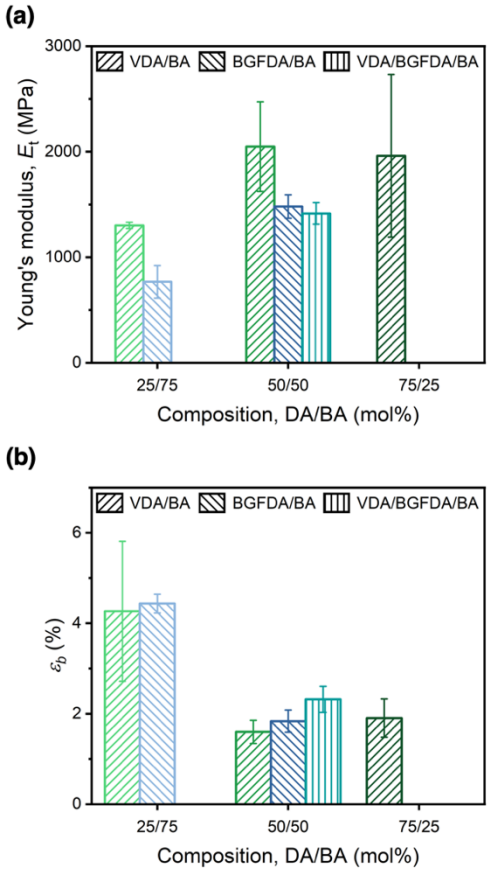

Fig. 4 (a) Young's modulus (E_t) and (b) elongation at break (ε_b) of acrylate networks. Error bars represent the standard deviations from triplicate measurements.

5 CONCLUSIONS

This work examined engineering strategies utilizing the composition and aromatic content of lignin-derivable diacrylates as tuning handles to investigate thermomechanical properties of a bio-derivable and processable vinyl ester resin platform. We demonstrated that the content of diacrylate incorporated in the network is the driving factor for tailoring both thermomechanical properties and network architecture. Specifically, increasing the amount of diacrylate led to an enhancement in E'_{25} due to a denser structure and higher extent of inhomogeneity attributed to the presence of more unreacted groups and non-uniformly distributed junctions that result in multiple

thermal relaxation modes. Additionally, the shift from monophenolic to bisphenolic diacrylate in binary component networks reduced the E'_{25} due to a slightly looser network achieved with larger diacrylate unit. Notably, a ternary network with mixed diacrylate types generated a network with a biphasic-like thermal relaxation mode and the highest extent of network inhomogeneity due to the formation of two distinct microphases. A deconvolution study of tan δ curves probed the highly inhomogeneous nature of a densely crosslinked system composed of bulky aromatic precursors. While all networks were highly inhomogeneous, these renewable acrylate networks showed tunable and comparable E'_{25} (~1-3 GPa) to petroleum-based acrylates, displaying potential for use in traditional composites, as well as broad tan δ curves harnessed from defects, further expanding their application to damping materials. Overall, this work showcased a design strategy through network engineering for processable, renewable vinyl ester resins exploiting the rigidity of lignin-derivable (bis)phenols and the low viscosity of a bio-derivable, aliphatic oil to tailor thermomechanical performance.

NOTES

The authors declare no competing financial interest.

ORCID

Yu-Tai Wong (orcid.org/0009-0001-3649-1361)

LaShanda T. J. Korley (orcid.org/0000-0002-8266-5000)

ACKNOWLEDGEMENTS

This work was supported by a National Science Foundation grant (NSF GCR CMMI 1934887) awarded to L. T. J. K. The authors thank the University of Delaware (UD) Advanced Materials Characterization Laboratory for the use of the ATR-FTIR, DSC, TGA, and SAXS

instruments, the UD NMR facility and UD Mass Spectrometry facility for the use of NMR and Mass Spectrometers, and Dr. Zachary Hinton and Dr. Daseul Jang for data analysis discussions. This research was also supported as part of the Center for Plastics Innovation, an Energy Frontier Research Center funded by the U.S. Department of Energy, Office of Science, Basic Energy Sciences, under award DE-SC0021166, for the use of the RSA-G2 instrument.

REFERENCES

1 J. S. Mahajan, R. M. O'Dea, J. B. Norris, L. T. J. Korley and T. H. Epps, *ACS Sustain. Chem. Eng.*, 2020, **8**, 15072–15096.
2 A. Llevot, E. Grau, S. Carlotti, S. Grelier and H. Cramail, *Macromol. Rapid Commun.*, 2016, **37**, 9–28.
3 V. Schimpf, A. Asmacher, A. Fuchs, K. Stoll, B. Bruchmann and R. Mülhaupt, *Macromol. Mater. Eng.*, 2020, **305**, 2000210.
4 C. N. Bowman and C. J. Kloxin, *Angew. Chem. Int. Ed.*, 2012, **51**, 4272–4274.
5 E. Feghali, K. M. Torr, D. J. van de Pas, P. Ortiz, K. Vanbroekhoven, W. Eevers and R. Vendamme, *Top. Curr. Chem.*, 2018, **376**, 32.
6 R. M. O'Dea, P. A. Pranda, Y. Luo, A. Amitrano, E. O. Ebikade, E. R. Gottlieb, O. Ajao, M. Benali, D. G. Vlachos, M. Ierapetritou and T. H. Epps, *Sci. Adv.*, 2022, **8**, eabj7523.
7 S. Zhao, X. Huang, A. J. Whelton and M. M. Abu-Omar, *ACS Sustain. Chem. Eng.*, 2018, **6**, 7600–7608.
8 J. F. Stanzione, J. M. Sadler, J. J. La Scala and R. P. Wool, *ChemSusChem*, 2012, **5**, 1291–1297.
9 S. K. Yadav, K. M. Schmalbach, E. Kinaci, J. F. Stanzione and G. R. Palmese, *Eur. Polym. J.*, 2018, **98**, 199–215.
10 M. K. Porwal, M. M. Hausladen, C. J. Ellison and T. M. Reineke, *Green Chem.*, 2023, **25**, 1488–1502.
11 A. V. Krishnan, P. Stathis, S. F. Permuth, L. Tokes and D. Feldman, *Endocrinology*, 1993, **132**, 2279–2286.
12 N. Olea, R. Pulgar, P. Pérez, F. Olea-Serrano, A. Rivas, A. Novillo-Fertrell, V. Pedraza, A. M. Soto and C. Sonnenschein, *Environ. Health Perspect.*, 1996, **104**, 298–305.
13 S. Takayanagi, T. Tokunaga, X. Liu, H. Okada, A. Matsushima and Y. Shimohigashi, *Toxicol. Lett.*, 2006, **167**, 95–105.
14 J. F. Stanzione III, J. M. Sadler, J. J. La Scala, K. H. Reno and R. P. Wool, *Green Chem.*, 2012, **14**, 2346.
15 J. F. Stanzione, P. A. Giangiulio, J. M. Sadler, J. J. La Scala and R. P. Wool, *ACS Sustain. Chem. Eng.*, 2013, **1**, 419–426.
16 Y. Zhang, Y. Li, L. Wang, Z. Gao and M. R. Kessler, *ACS Sustain. Chem. Eng.*, 2017, **5**, 8876–8883.

17 B. T. White, V. Meenakshisundaram, K. D. Feller, C. B. Williams and T. E. Long, *Polymer*, 2021, **223**, 123727.
18 R. M. O'Dea, J. A. Willie and T. H. Epps, *ACS Macro Lett.*, 2020, **9**, 476–493.
19 P. J. De Wild, W. J. J. Huijgen and R. J. A. Gosselink, *Biofuels Bioprod. Biorefining*, 2014, **8**, 645–657.
20 A. Tolbert, H. Akinosho, R. Khunsupat, A. K. Naskar and A. J. Ragauskas, *Biofuels Bioprod. Biorefining*, 2014, **8**, 836–856.
21 W. Schutyser, T. Renders, S. Van den Bosch, S.-F. Koelewijn, G. T. Beckham and B. F. Sels, *Chem. Soc. Rev.*, 2018, **47**, 852–908.
22 A. Vishtal and A. Kraslawski, *BioResources*.
23 V. K. Thakur, M. K. Thakur, P. Raghavan and M. R. Kessler, *ACS Sustain. Chem. Eng.*, 2014, **2**, 1072–1092.
24 G. F. Bass and T. H. Epps, *Polym. Chem.*, 2021, **12**, 4130–4158.
25 G. Yang, B. J. Rohde, H. Tesefay and M. L. Robertson, *ACS Sustain. Chem. Eng.*, 2016, **4**, 6524–6533.
26 A. Amitrano, J. S. Mahajan, L. T. J. Korley and T. H. Epps, *RSC Adv.*, 2021, **11**, 22149–22158.
27 Y. Peng, K. H. Nicastro, T. H. Epps, III and C. Wu, *Food Chem.*, 2021, **338**, 127656.
28 S. V. Mhatre, J. S. Mahajan, T. H. Epps and L. T. J. Korley, *Mater. Adv.*, 2023, **4**, 110–121.
29 K. H. Nicastro, C. J. Kloxin and T. H. Epps, *ACS Sustain. Chem. Eng.*, 2018, **6**, 14812–14819.
30 M. Fache, B. Boutevin and S. Caillol, *Eur. Polym. J.*, 2015, **68**, 488–502.
31 A. L. Holmberg, N. A. Nguyen, M. G. Karavolias, K. H. Reno, R. P. Wool and T. H. Epps, *Macromolecules*, 2016, **49**, 1286–1295.
32 A. L. Holmberg, K. H. Reno, N. A. Nguyen, R. P. Wool and T. H. Epps, *ACS Macro Lett.*, 2016, **5**, 574–578.
33 S. Cousinet, A. Ghadban, E. Fleury, F. Lortie, J.-P. Pascault and D. Portinha, *Eur. Polym. J.*, 2015, **67**, 539–550.
34 M. Fache, E. Darroman, V. Besse, R. Auvergne, S. Caillol and B. Boutevin, *Green Chem*, 2014, **16**, 1987–1998.
35 C. Veith, F. Diot-Néant, S. A. Miller and F. Allais, *Polym. Chem.*, 2020, **11**, 7452–7470.
36 E. D. Hernandez, A. W. Bassett, J. M. Sadler, J. J. La Scala and J. F. Stanzione, *ACS Sustain. Chem. Eng.*, 2016, **4**, 4328–4339.
37 C. Zhang, S. A. Madbouly and M. R. Kessler, *Macromol. Chem. Phys.*, 2015, **216**, 1816–1822.
38 A. W. Bassett, C. M. Breyta, A. E. Honnig, J. H. Reilly, K. R. Sweet, J. J. La Scala and J. F. Stanzione, *Eur. Polym. J.*, 2019, **111**, 95–103.
39 A. W. Bassett, A. E. Honnig, C. M. Breyta, I. C. Dunn, J. J. La Scala and J. F. Stanzione, *ACS Sustain. Chem. Eng.*, 2020, **8**, 5626–5635.
40 R. Anastasio, R. Cardinaels, G. W. M. Peters and L. C. A. Breemen, *J. Appl. Polym. Sci.*, 2020, **137**, 48498.
41 M. Podgórski, *J. Appl. Polym. Sci.*, 2009, **112**, 2942–2952.
42 A. M. Ortega, S. E. Kasprzak, C. M. Yakacki, J. Diani, A. R. Greenberg and K. Gall, *J. Appl. Polym. Sci.*, 2008, **110**, 1559–1572.
43 L. Rey, J. Duchet, J. Galy, H. Sautereau, D. Vouagner and L. Carrion, *Polymer*, 2002, **43**, 4375–4384.
44 S. Seiffert, *Polym. Chem.*, 2017, **8**, 4472–4487.
45 A. Jangizehi, F. Schmid, P. Besenius, K. Kremer and S. Seiffert, *Soft Matter*, 2020, **16**, 10809–10859.

46 Y. Gu, J. Zhao and J. A. Johnson, *Angew. Chem. Int. Ed.*, 2020, **59**, 5022–5049.
47 H. Zhou, J. Woo, A. M. Cok, M. Wang, B. D. Olsen and J. A. Johnson, *Proc. Natl. Acad. Sci.*, 2012, **109**, 19119–19124.
48 M. Zhong, R. Wang, K. Kawamoto, B. D. Olsen and J. A. Johnson, *Science*, 2016, **353**, 1264–1268.
49 N. J. Rebello, H. K. Beech and B. D. Olsen, *ACS Macro Lett.*, 2021, **10**, 531–537.
50 C.-L. Qin, W.-M. Cai, J. Cai, D.-Y. Tang, J.-S. Zhang and M. Qin, *Mater. Chem. Phys.*, 2004, **85**, 402–409.
51 D. Ratna, V. G. Dalvi, S. Billa, S. K. Sharma, S. K. Rath, K. Sudarshan and P. K. Pujari, *ACS Appl. Polym. Mater.*, 2021, **3**, 5073–5086.
52 E. Penzel, N. Ballard and J. M. Asua, in *Ullmann's Encyclopedia of Industrial Chemistry*, Wiley-VCH Verlag GmbH & Co. KGaA, Weinheim, Germany, 2018, pp. 1–20.
53 C. Kim, A. Chandrasekaran, T. D. Huan, D. Das and R. Ramprasad, *J. Phys. Chem. C*, 2018, **122**, 17575–17585.
54 C. Kuenneth, W. Schertzer and R. Ramprasad, *Macromolecules*, 2021, **54**, 5957–5961.
55 A. Shundo, M. Aoki, P. Wang, T. Hoshino, S. Yamamoto, S. Yamada and K. Tanaka, *Macromolecules*, 2023, **56**, 3884–3890.

Supporting Information (SI)

Engineering lignin-derivable diacrylate networks with tunable architecture and mechanics

*Yu-Tai Wong[1], LaShanda T. J. Korley[1,2]**

[1]Department of Chemical and Biomolecular Engineering, University of Delaware, Newark, Delaware 19716, United States

[2]Department of Materials Science and Engineering, University of Delaware, Newark, Delaware 19716, United States

*Corresponding author, E-mail: lkorley@udel.edu

Abbreviations

BGF	Bisguaiacol F
BGFDA	Bisguaiacol F diacrylate
BA	*n*-butyl acrylate
DCM	Dichloromethane
E_t	Young's modulus
$T_{d,5\%}$	Degradation temperature at 5 wt% loss
T_g	Glass transition temperature
VDA	Vanillyl alcohol diacrylate
ε_B	Elongation-at-break
σ_M	Ultimate tensile strength

Proton (^{1}H) Nuclear Magnetic Resonance (NMR) spectra for lignin-derivable building blocks in deuterated chloroform ($CDCl_3$)

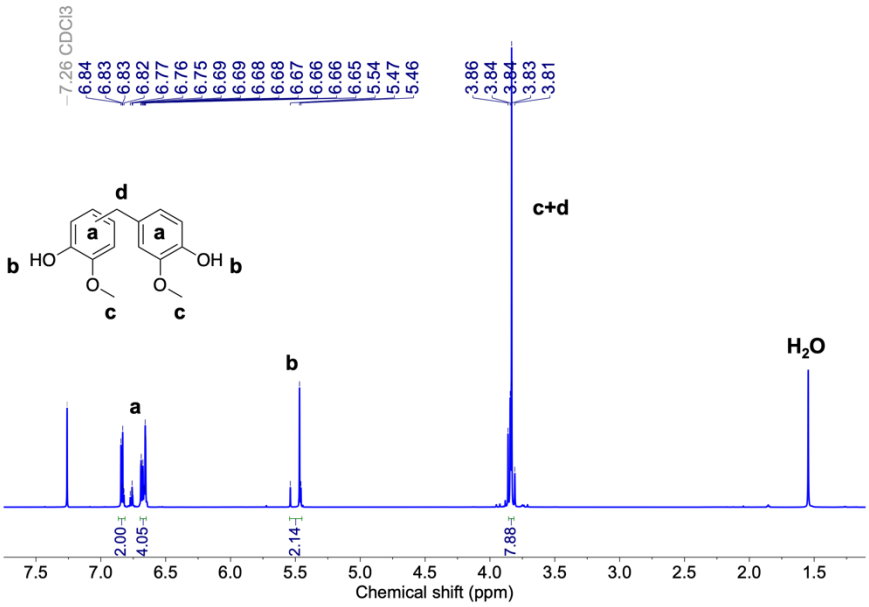

Fig. S1 ^{1}H NMR spectrum of bisguaiacol F

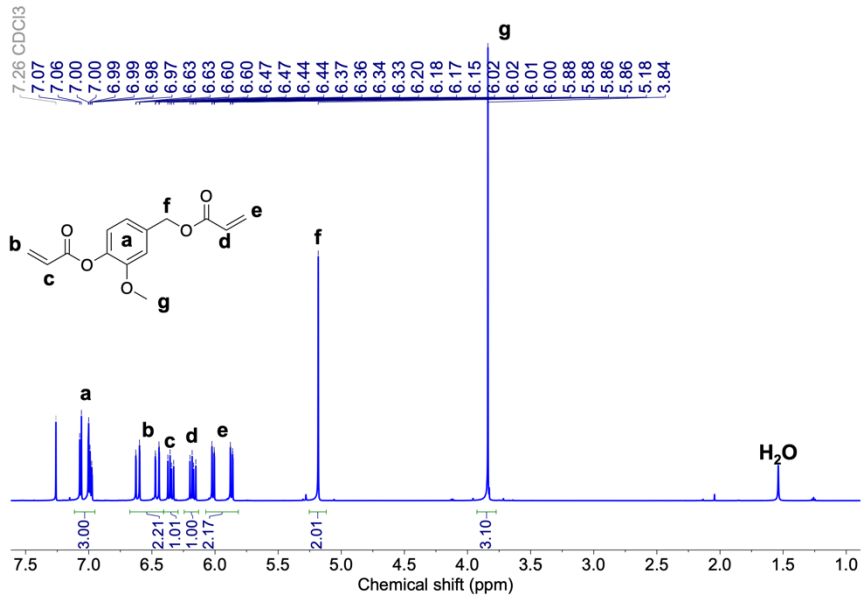

Fig. S2 ^{1}H NMR spectrum of vanillyl alcohol diacrylate

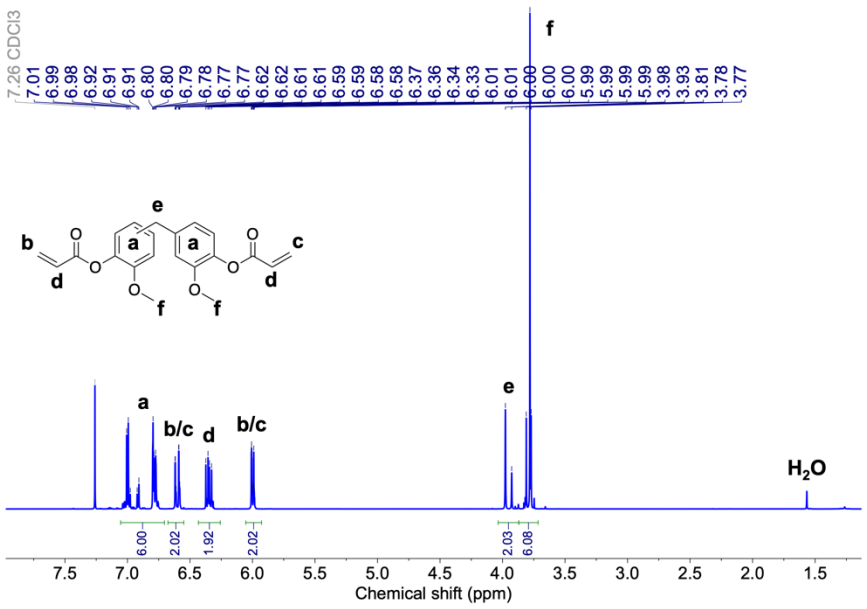

Fig. S3 ^{1}H NMR spectrum of bisguaiacol F diacrylate

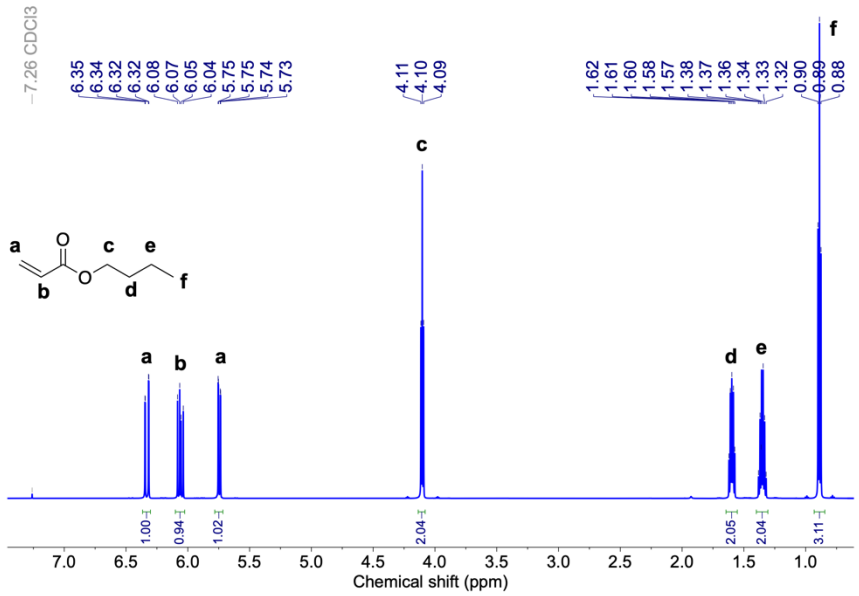

Fig. S4 ^{1}H NMR spectrum of *n*-butyl acrylate

Film curing steps and film appearances

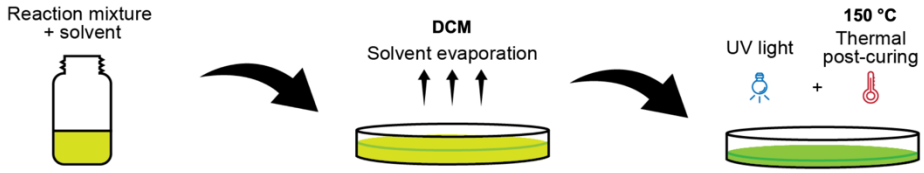

Fig. S5 Schematic representation of film casting and curing procedures

Fig. S6 Optical images of each acrylate networks after thermal post-curing with a film thickness ~0.2 mm

Differential scanning calorimetry (DSC) results for curing of acrylate networks

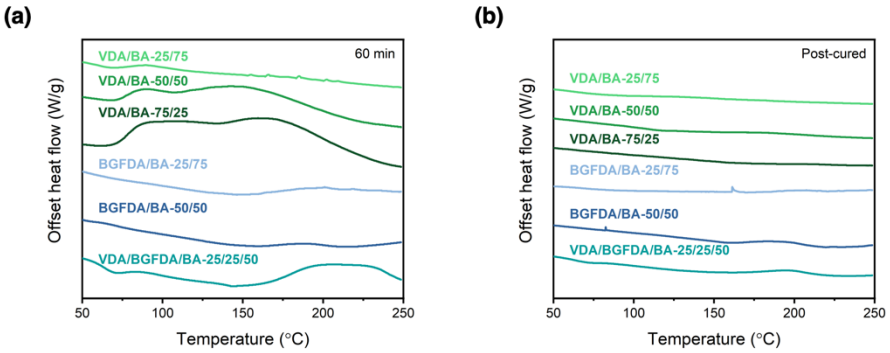

Fig. S7 DSC curve of acrylate networks (a) before and (b) after thermal post-curing (exotherm up, 10 °C/min, N_2). Exothermic peaks in (a) were applied to determine the temperature for thermal post-curing.

Attenuated total reflectance-Fourier transform infrared (ATR-FTIR) spectra for acrylate networks

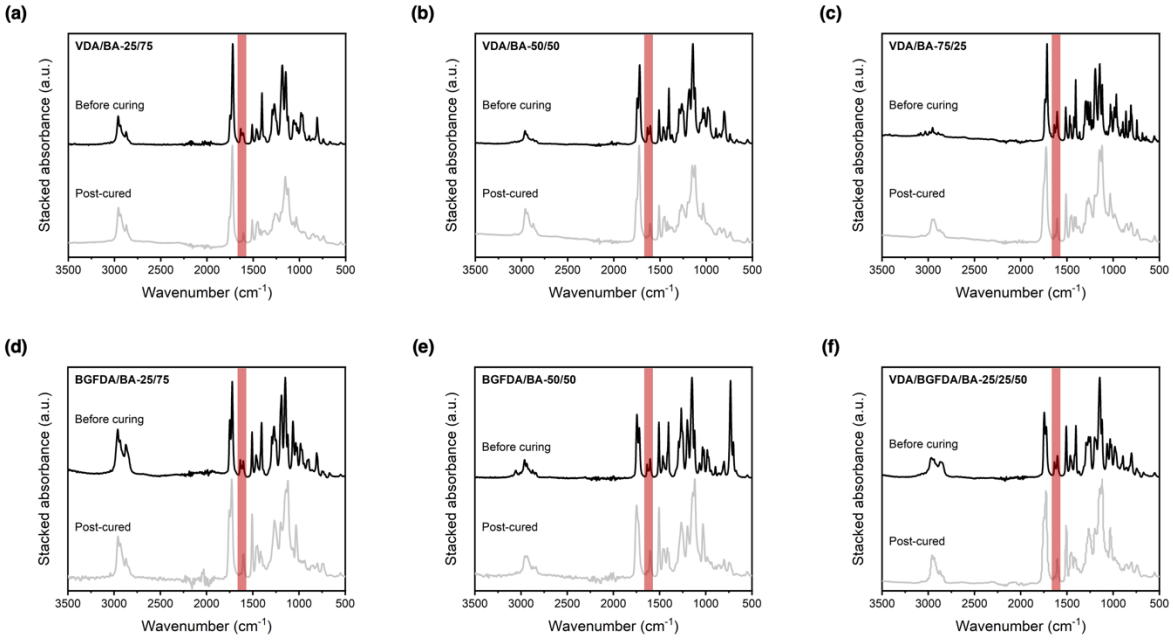

Fig. S8 Stacked ATR-FTIR spectra of acrylate networks before and after thermal post-curing. The conversion was probed quantitatively by the disappearance of the acrylate carbon double bond stretching band at ~1635 cm^{-1} (highlighted in red) with an internal reference of carbonyl double bond stretching band at ~1724 cm^{-1} (128 scans, resolution 4 cm^{-1}).

Thermogravimetric analysis (TGA) results of acrylate networks

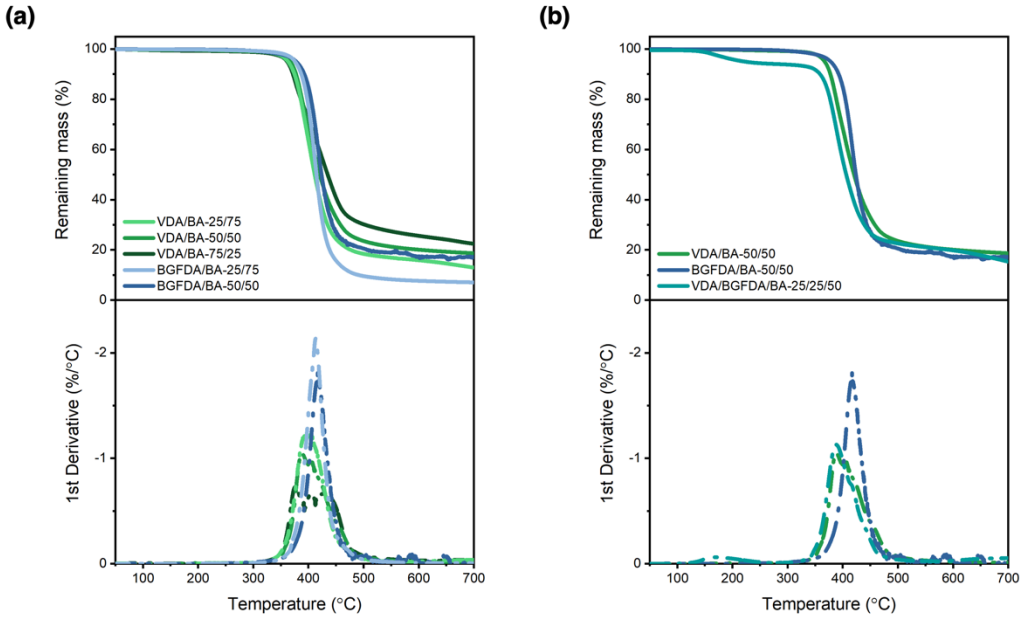

Fig. S9 Thermogravimetric analysis traces and respective first-derivative curves of acrylate networks for (a) varying diacrylate content and (b) varying diacrylates (10 °C/min, N_2).

Table S1 $T_{d,5\%}$ of acrylate networks.

Sample	$T_{d,5\%}$ (°C)
VDA/BA-25/75	363
VDA/BA-50/50	367
VDA/BA-75/25	361
BGFDA/BA-25/75	376
BGFDA/BA-50/50	378
VDA/BGFDA/BA-25/25/50	222

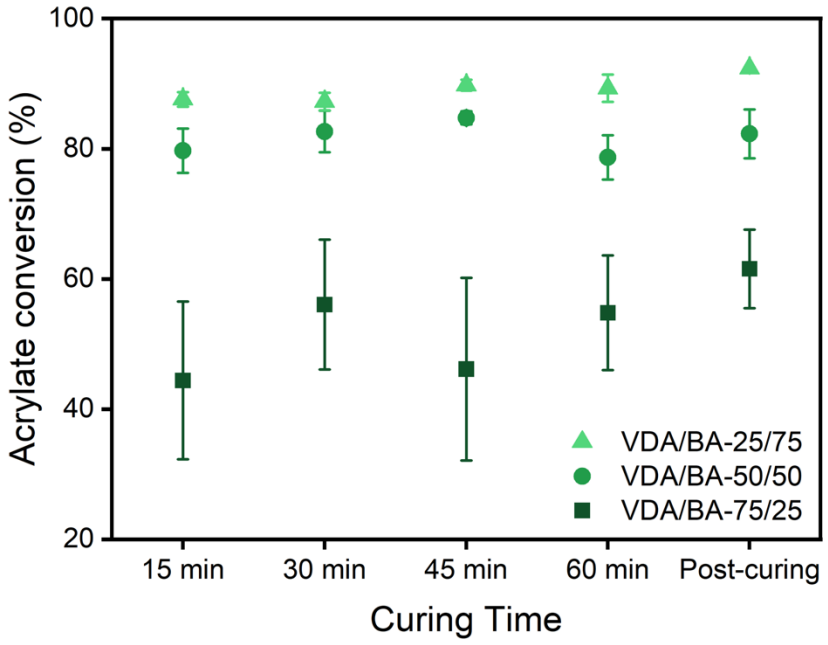

Fig. S10 Conversion profile of VDA/BA networks at different curing times as an example of the evolution of network formation. Each data point represents the triplicated result using samples from different batch.

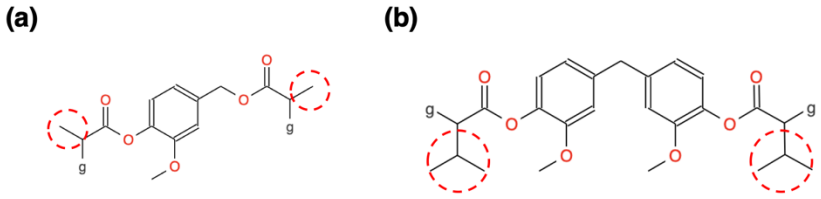

Fig. S11 Structures used to predict T_gs of the homopolymer for (a) VDA and (b) BGFDA *via* Polymer Genome. 'g' represents the bond with repeated units, and side groups marked with red dashed circle denote the structure added manually to mimic crosslinked structure. The predicted T_g for VDA homopolymer is 194 °C and BGFDA homopolymer is 222 °C.

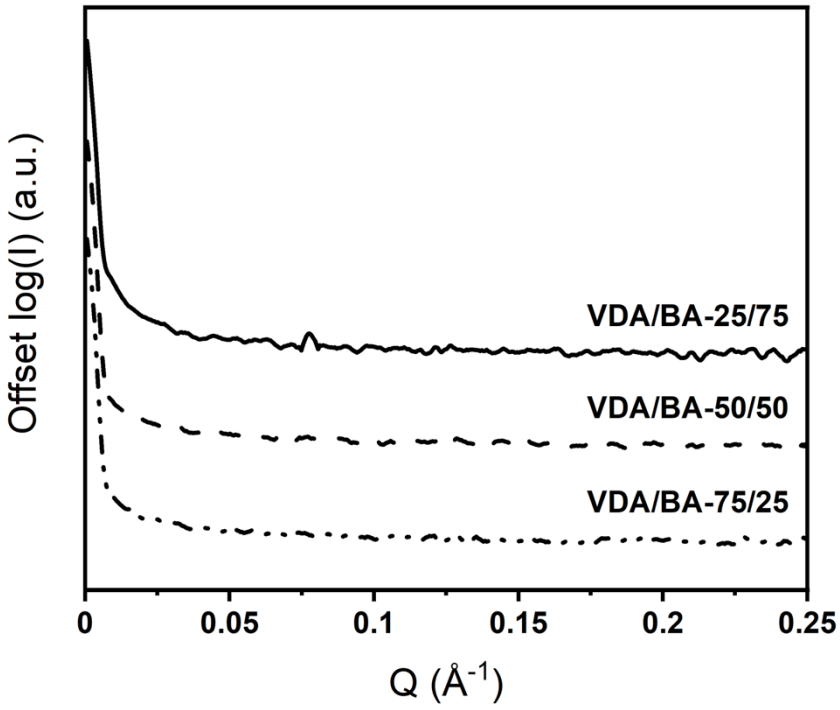

Fig. S12 Small-angle X-ray scattering spectra for VDA/BA networks. Curves are based on absolute scale and shifted vertically for clarity (sample-to-detector distance: 1200 mm).

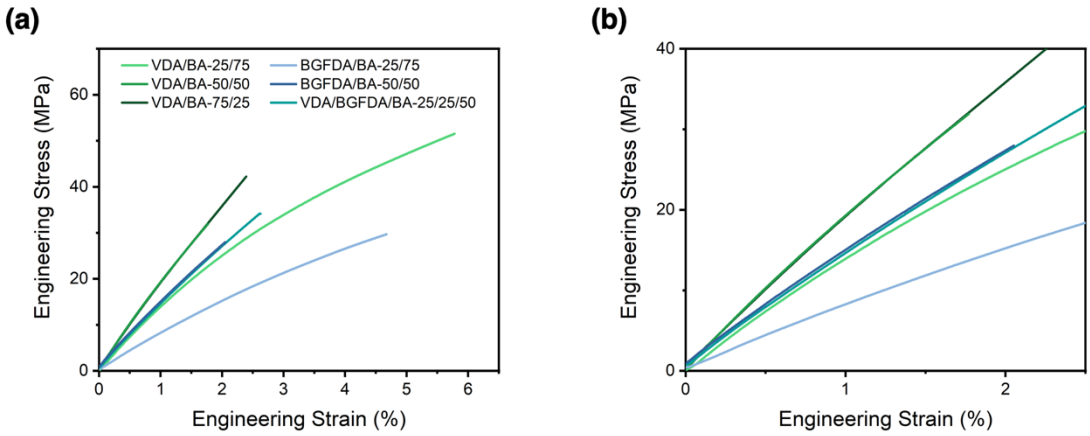

Fig. S13 Uniaxial tensile curves of acrylate networks for (a) full scale and (b) scale in the low strain region.

Table S2 Uniaxial tensile properties of acrylate networks

	E_t (GPa)	ε_B (%)	σ_M(MPa)	Toughness (MJ m^{-3})
VDA/BA-25/75	1.3 ± 0.1	4.3 ± 1.6	40.6 ± 6.3	1.1 ± 0.5
VDA/BA-50/50	2.0 ± 0.4	1.6 ± 0.3	28.8 ± 4.0	0.3 ± 0.1
VDA/BA-75/25	2.0 ± 0.8	1.9 ± 0.4	32.6 ± 5.8	0.3 ± 0.1
BGFDA/BA-25/75	0.8 ± 0.2	4.4 ± 0.2	28.6 ± 1.2	0.7 ± 0.1
BGFDA/BA-50/50	1.5 ± 0.1	1.8 ± 0.3	25.4 ± 1.5	0.3 ± 0.1
VDA/BGFDA/BA-25/25/50	1.4 ± 0.1	2.3 ± 0.3	30.7 ± 3.3	0.4 ± 0.1